Applied Catalysis B: Environmental 142–143 (2013) 406–413

Contents lists available at SciVerse ScienceDirect

Applied Catalysis B: Environmental

journal homepage: www.elsevier.com/locate/apcatb

Effect of catalyst composition and preparation conditions on catalytic properties of unsupported manganese oxides for benzene oxidation with ozone

Hisahiro Einaga*, Nanako Maeda, Yasutake Teraoka

Department of Energy and Material Sciences, Faculty of Engineering Sciences, Kyushu University, Kasuga, Fukuoka 816-8580, Japan

ARTICLE INFO

Article history:
Received 9 March 2013
Received in revised form 15 May 2013
Accepted 21 May 2013
Available online 29 May 2013

Keywords:
Catalytic oxidation
Ozone
Manganese oxides
Manganese-containing mixed oxides

ABSTRACT

Catalytic oxidation of benzene in gas phase with ozone was carried out at 70 °C over manganese oxides and manganese-based mixed oxides to investigate the effect of catalyst composition and preparation conditions on their catalytic properties. The oxides were prepared by an evaporation-to-dryness method and a co-precipitation method from metal nitrate precursors, followed by calcination at 400–900 °C. As for manganese monoxides, benzene oxidation rate normalized by catalyst surface area, product distribution and ozone/benzene decomposition ratio were almost independent of the preparation method and calcination temperature. Perovskite-type mixed oxides, $LaMnO_3$ and $La_{0.8}Sr_{0.2}MnO_3$ showed much lower activity and lower efficiency for ozone utilization in benzene oxidation than manganese monoxide and La sites promoted the accumulation of less-reactive byproduct compounds on the catalysts. In the case of manganese-based mixed oxides that contained Fe, Co, Ni, and Cu, benzene oxidation activity, CO_2 selectivity and ozone/benzene decomposition ratio depended on the catalyst composition and preparation conditions. Among the mixed oxide catalysts, the Co–Mn mixed oxide prepared by the evaporation-to dryness method and calcined at 400 °C was the most effective for benzene oxidation from the standpoint of CO_2 selectivity and efficiency for ozone utilization.

1. Introduction

Control of air quality has been one of the important environmental issues over the past decades. Catalytic oxidation by using ozone (catalytic ozonation) is one of the effective processes for abatement of volatile organic compounds (VOCs) in gas phase especially at their low concentration levels [1]. The catalytic ozonation processes have an advantage over catalytic combustion processes in that inexpensive metals in the first transition series, such as manganese can be used as the active species for the reaction. The addition of ozone decreases the reaction temperature required for benzene oxidation on manganese oxides and the apparent activation energy, as compared with catalytic combustion [2]. So far, supported and unsupported manganese oxide catalysts have been used for complete oxidation of various kinds of organic compounds [2–17], and they exhibited higher activity for the oxidation of benzene and cyclohexane than the oxides of transition metals in the first transition series, Fe, Co, Ni and Cu [18].

For the practical application of catalytic ozonation processes, catalyst design is important from the standpoint of efficiency for VOC removal because the VOC oxidation rate, product distribution and efficiency for ozone utilization depend on the catalyst materials used in the reaction. One of the effective methods for improving the catalytic properties of manganese oxides is to increase the catalyst surface area by depositing manganese oxides on supporting materials with high surface area. We have investigated the effect of manganese oxide structures and the kinds of supports on the catalytic properties for benzene oxidation with ozone [19,20]. Benzene oxidation rate with supported manganese oxides strongly depended on the catalyst surface area and was almost independent of the kinds of catalyst supports [20]. Manganese oxides supported on SiO_2 with high-surface area were thus one of the promising catalysts for catalytic ozonation of benzene.

Another method for improving the catalytic properties of manganese oxides involves their combination with other kinds of metal oxides. It has been reported that catalytic oxidation ability is higher for manganese-containing mixed oxides than the single oxides due to the changes in the oxidation state of manganese [21] and the increase in catalyst surface area [22]. In the case of catalytic ozonation processes, the mixed oxides of these transition metals have been also used for the reaction. Comparison of the catalytic properties of $NiMnO_3$ ilmenite and $NiMn_2O_4$ spinel revealed that the

* Corresponding author. Tel.: +81 92 583 7525; fax: +81 92 583 8853.
E-mail address: einaga.hisahiro.399@m.kyushu-u.ac.jp (H. Einaga).

0926-3373/$ – see front matter © 2013 Elsevier B.V. All rights reserved.
http://dx.doi.org/10.1016/j.apcatb.2013.05.041

former mixed oxides exhibited higher activity for benzene oxidation [11]. Other kinds of mixed metal oxides have been also used for catalytic ozonation processes [23].

In this study, we carried out benzene oxidation with ozone over manganese-based monoxides and mixed oxides to investigate the effect of catalyst composition and preparation methods on their properties. The catalytic properties were compared from the standpoint of catalytic activity, CO_2 selectivity and efficiency for ozone utilization, which are the important characters for high-performance catalysts in catalytic ozonation processes.

2. Experimental

2.1. Catalyst preparation

All reagents were analytical grade and used without further purification. Manganese oxides and manganese-containing mixed oxides were mainly prepared by an evaporation-to-dryness method. Aqueous solutions of metal nitrates and malic acid were dissolved into pure water in a molar ratio of 2:3. The solution was heated under vigorous stirring and evaporated to dryness. The residual was ground well with a pestle and mortar and calcined at the temperature of 400–900 °C to obtain the final products. This method is denoted by Amorphous Malate Precursor (AMP) method. Metal oxides were also prepared by a co-precipitation method. An aqueous solution of metal nitrate was dropped into aqueous ammonia solution (25%) or the aqueous solution containing $NaHCO_3$ under vigorous stirring. The resulting precipitates were filtrated, washed with pure water, dried at 373 K and calcined at the temperature of 400–600 °C. This method is denoted by Reverse Homogeneous Precipitation (RHP) method.

2.2. Catalyst characterization

The catalysts were characterized by powder XRD using a RIGAKU RINT2200 diffractometer with Cu Kα radiation. Catalyst surface area was determined by BET method from N_2 adsorption isotherm at 77 K. FTIR spectra of the catalysts were obtained by using Jasco FTIR 480 Plus spectrometer equipped with a diffuse reflectance accessory (Jasco DR-81). EXAFS measurements were carried out at the Kyushu Synchrotron Light Research Center (SAGA-LS) beam line BL06 with the storage ring operating at an energy of 1.4 GeV. Catalyst samples were mixed with boron nitride (BN) and pressed into thin disks (20 mm ϕ). EXAFS spectra were recorded at room temperature. Data reduction of experimental absorption spectra was carried out according to the method recommended by the Standards and Criteria Committee of the International XAFS Society [24] using a REX2000 software.

2.3. Catalytic reactions

Catalytic ozonation of benzene was carried out with a fixed bed flow reactor. Details of the reaction system for benzene oxidation were reported in the previous papers [19,20]. Reaction gases for the catalytic reactions were prepared by mixing benzene in N_2, N_2 (> 99.9995%, total hydrocarbon < 1 ppm) and O_2 (>99.9995%, total hydrocarbon < 1 ppm) in cylinders. Ozone was synthesized from pure O_2 by using an ozone generator. Prior to the benzene oxidation with ozone, catalyst was heated at 300 °C in O_2 flow for 1 h, and then thermostatted at a reaction temperature (70 or 100 °C) with a water bath or a heating apparatus. Inlet concentration: benzene 150 ppm, ozone 2250 ppm, O_2 10%, gas flow rate 500 ml/min (N_2: 300 ml/min, C_6H_6: 150 ml/min, O_2: 50 ml/min), catalyst weight 0.10–0.20 g. Gas sample was analyzed by using a FTIR spectrometer (Perkin-Elmer Spectrum One) equipped with a 2.4 m optical length gas cell (volume 100 ml). In this system, homogeneous gaseous reaction of benzene with ozone can be neglected [19,20]. Catalytic benzene oxidation was also carried out without ozone feed by using the same reaction system.

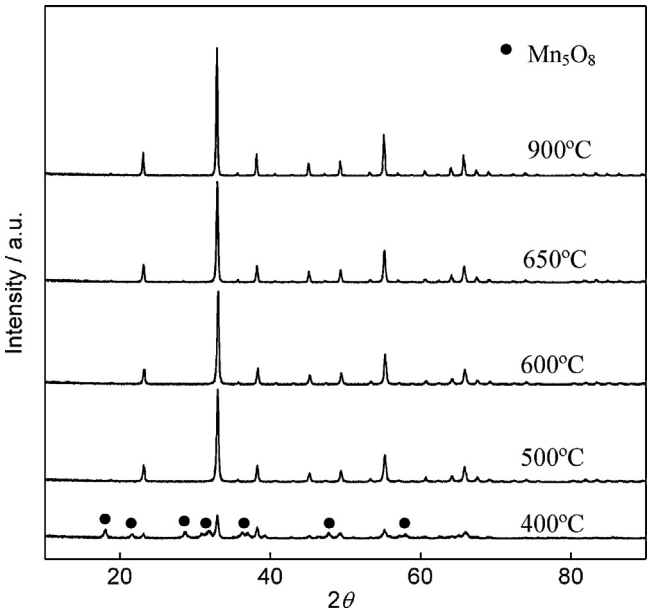

Fig. 1. XRD patterns of manganese oxides prepared by AMP method and calcined at different temperatures.

3. Results and discussion

3.1. Effect of preparation conditions on catalytic properties of manganese oxides

The structure of Mn oxides strongly depended on the preparation method and calcination temperature. Fig. 1 shows the XRD patterns of Mn oxides prepared by evaporation-to-dryness technique and calcined at various temperatures. Mn oxides calcined at 400 °C showed small peaks of Mn_2O_3 and Mn_5O_8 structures. Upon the rising in the calcination temperature, the Mn_5O_8 phase diminished and the peak intensities for Mn_2O_3 greatly increased, indicating that the degree of crystallinity increased.

Fig. 2 shows benzene oxidation behavior on the Mn oxide catalysts calcined at various temperatures. The catalyst surface area decreased with the increase of calcination temperature (Fig. 2(a)) due to the increase in the degree of crystallinity. Benzene oxidation rate linearly increased with the increase in catalyst surface area (Fig. 2(b)). The amount of CO_2 and CO formed was equal to that of benzene reacted, showing that carbon balance was almost perfect for all the catalysts (Fig. 2(c)). In addition, no organic byproducts were detected in gas phase. The mole fractions of CO_2 and CO were around 75% and 25%, and they were almost independent of benzene conversion (Fig. 2(d)). The ozone/benzene decomposition ratio was estimated to be 15 and did not change when the calcination temperature of Mn oxide catalysts were variously changed (Fig. 2(e)). These results indicate that the catalyst surface area of Mn monoxides is one of the important factors controlling their catalytic activity, whereas other catalytic properties of Mn oxides such as product distribution are not so much affected by the changes in catalyst surface area and Mn oxide structures.

It has been reported that ozone is decomposed on Mn oxide catalysts to form oxygen species (Eqs. (1)–(4)), which takes part in oxidation of organic compounds on the catalysts [3–8].

$$O_3 + * \rightarrow O_2 + O* \quad (1)$$

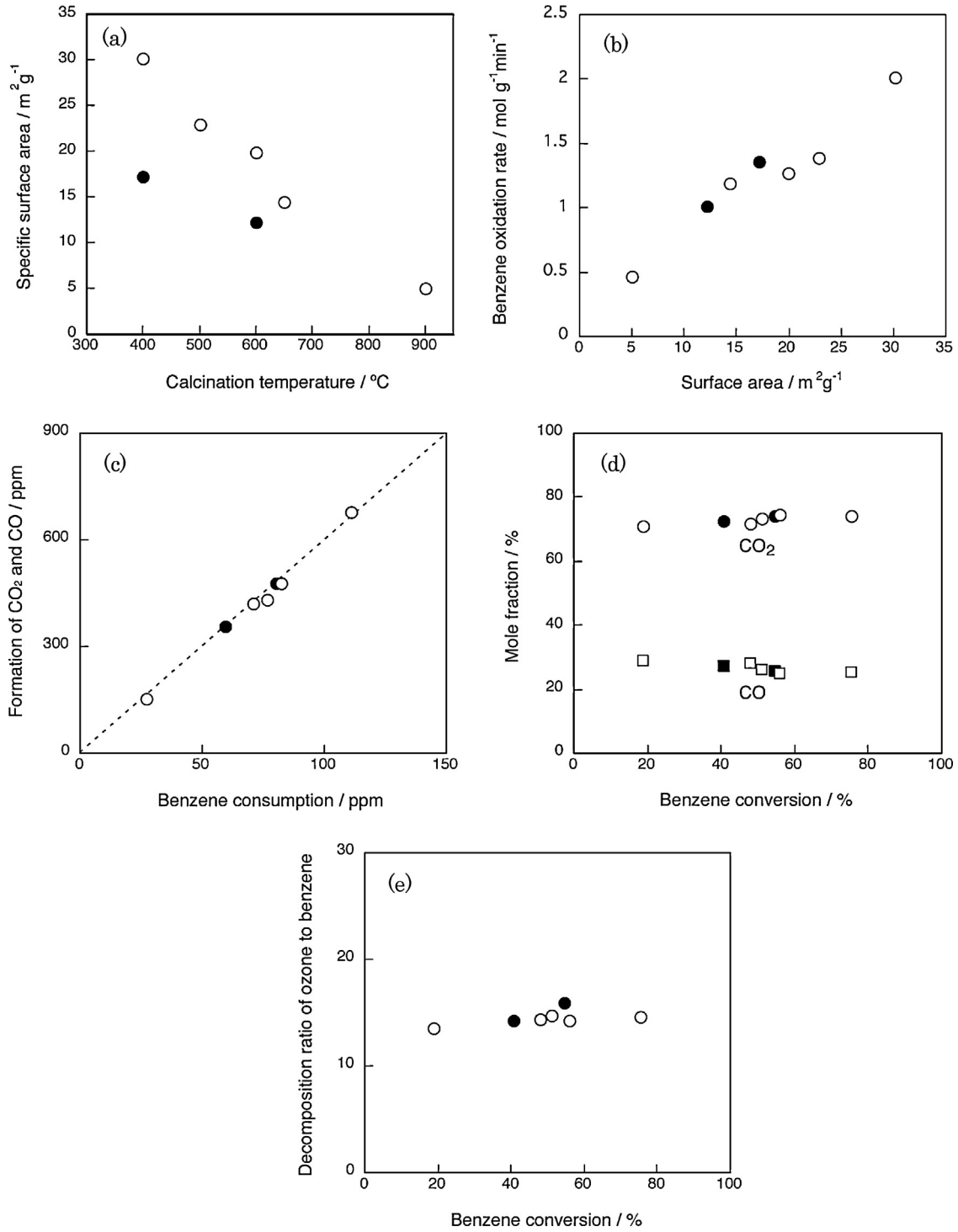

Fig. 2. Benzene oxidation behavior over manganese oxides with ozone. (a) Effect of catalyst calcination temperature on catalyst surface area. (b) Relationship between catalyst surface area and benzene oxidation rate. (c) Relationship between benzene consumption and CO_x formation. (d) Relationship between benzene conversion and mole fraction of CO_2 and CO, (e) Plots of decomposition ratio of ozone to ratio against benzene conversion. Open symbols (○,□) refer to the catalyst prepared by AMP method and closed symbols (●,■) to that by RHP method. Catalyst 0.10 g, inlet concentration: benzene 150 ppm, O_3 2250 ppm, O_2 10%, gas flow rate 500 ml/min, reaction temperature 70 °C.

$$O* + O_3 \rightarrow O_2 + O_2* \quad (2)$$

$$O_2* \rightarrow O_2 + * \quad (3)$$

$$O* + C_6H_6 \rightarrow \text{decomposition} \quad (4)$$

(* refers to the catalyst active sites)

On the basis of this reaction mechanism, we can discuss the efficiency for ozone utilization in catalytic benzene oxidation. When one oxygen atom of ozone is reacted with the organic compounds, the reaction stoichiometry is expressed by the following equation (Eq. (5)).

$$C_6H_6 + (15-x)O_3 \rightarrow (6-x)CO_2 + xCO + (15-x)O_2 + 3H_2O \quad (5)$$

Table 1
Catalytic properties of manganese oxides prepared by RHP method.[a]

Alkaline reagent	Calcination temperature (°C)	Surface area ($m^2\ g^{-1}$)	Benzene oxidation rate ($\times10^{-5}$ mol g^{-1} min)	CO mole fraction (%)	Ozone/benzene decomposition	Crystalline phase
$NaHCO_3$	400	20.4	2.0	16.4	17.5	Mn_5O_8
$NaHCO_3$	600	10.7	1.3	12.0	34.4	Mn_2O_3, $Na_2Mn_5O_{10}$
NH_3	400	17.8	1.4	25.7	16.0	Mn_5O_8
NH_3	600	12.1	1.0	27.5	14.3	Mn_2O_3

[a] Catalyst 0.10 g, inlet concentration: benzene 150 ppm, O_3 2250 ppm, O_2 10%, gas flow rate 500 ml/min, reaction temperature 70 °C.

Table 2
Catalytic properties of Mn_2O_3 and perovskite oxides.

Catalyst	Benzene oxidation without ozone[a] (mol min^{-1} m^{-2})	Benzene oxidation with ozone[b] (mol min^{-1} m^{-2})	Ozone Decomposition[c] (mol min^{-1} m^{-2})
Mn_2O_3	2.0×10^{-7}	8.3×10^{-7}	3.3×10^{-6}
$LaMnO_3$	2.8×10^{-7}	1.6×10^{-7}	2.8×10^{-6}

[a] Catalyst 0.10 g, benzene 400 ppm, O_2 20%, gas flow rate 100 ml/min, 200 °C.
[b] Catalyst 0.20 g, benzene 150 ppm, O_3 2250 ppm, O_2 10%, gas flow rate 500 ml/min, 70 °C.
[c] Catalyst 0.030 g, benzene 150 ppm, O_3 2250 ppm, O_2 10%, gas flow rate 500 ml/min., 70 °C.

In the case of Mn monoxide catalysts, ozone/benzene decomposition ratio, which was the character of the efficiency for ozone utilization was estimated to be 15 and was close to the value obtained from the stoichiometric equation (13.5 for $[CO_2]/[CO] = 3$). Therefore, benzene oxidation with ozone followed the stoichiometric equation, indicating that ozone was efficiently used in benzene oxidation. The ozone/benzene decomposition ratio was independent of the surface area and structure of Mn oxides, as described above.

We also investigated the effect of preparation methods for Mn oxides on the catalytic properties for benzene oxidation with ozone. The Mn oxide catalysts were prepared by the co-precipitation method using aqueous ammonia solution (RHP method) and calcined at 400 and 600 °C. The Mn oxides thus prepared have lower catalyst surface than those prepared by AMP method (Fig. 2(a)). However, the reaction rates normalized by surface area were comparable for the catalysts (Fig. 2(b)). In addition, product distribution (CO_x mole fractions) and the efficiency for ozone utilization (ozone/benzene decomposition ratio) were close to the values for Mn oxides prepared by AMP method (Fig. 2(c)–(e)). Thus, catalytic properties of Mn oxides were not affected by the preparation methods.

However, impurities in Mn oxide catalysts had great influence on their catalytic properties for benzene oxidation with ozone. Metal oxides are frequently prepared by co-precipitation methods using $NaHCO_3$ as the precipitant. The metal oxides prepared by this process have the tendency to contain impurities when the after treatment process (catalyst washing) is insufficient. In the present study, a typical result was obtained for Mn oxide catalysts and an impurity phase $Na_2Mn_5O_{10}$ was detected when $NaHCO_3$ was used the precipitant and washing processes were insufficient (Table 1). Although the catalyst surface area was comparable, benzene oxidation activity was low compared with the Mn oxides prepared by the co-precipitation method using aqueous ammonia. In addition, the ozone/benzene decomposition ratio greatly increased to 34.4, indicating that the side reaction, namely, self-decomposition of ozone (Eq. (6)) on the catalyst surface was promoted by the presence of impurity phases.

$$2O_3 \rightarrow 3O_2 \quad (6)$$

3.2. Comparison of catalytic properties of manganese-containing perovskite oxides with manganese monoxides

Catalytic properties of Mn monoxides were compared with those of Mn-containing perovskite oxides in Table 2. XRD patterns confirmed the formation of perovskite oxide phases for $LaMnO_3$ and $La_{0.8}Sr_{0.2}MnO_3$ prepared by evaporation-to-dryness methods and calcined at 650 °C (Fig. 3). Mn monoxides prepared by the same preparation method but without the use of La and Sr mainly have the structure of Mn_2O_3 phases. In the case of benzene oxidation without ozone, $LaMnO_3$ exhibited higher activity than Mn monoxides. The rates for ozone decomposition in the absence of VOC were not so much different for these catalysts. On the other hand, the addition of La had detrimental effects on the activities for benzene oxidation with ozone. Fig. 4 shows typical time courses for benzene oxidation over Mn oxide and Mn-containing perovskite oxides at 70 °C. After conversion decreased in the initial period, Mn_2O_3 showed steady state activity (Fig. 4(a)). On the other hand, benzene oxidation activity with $LaMnO_3$ significantly decreased during the reaction (Fig. 4(b)). The difference between the two catalysts was also prominent for the efficiency for ozone utilization. Fig. 4(c) compares time course plots for ozone/benzene decomposition ratio. In the case of Mn oxides, the ratio was about 15 and almost unchanged during the reaction, indicating that ozone was efficiently consumed during the reaction. With the $LaMnO_3$ catalyst, on the other hand, the ratio was 15 in the initial period and increased gradually up to 35 after 150 min reaction, indicating that the self-decomposition of ozone (Eq. (6)) proceeded as the reaction time increased.

Table 3 compares the catalytic activities of Mn monoxides and Mn-containing perovskite oxides at higher W/F values than those in Fig. 4. The catalytic activity of $LaMnO_3$ increased with the rising in reaction temperature up to 100 °C. It has been reported

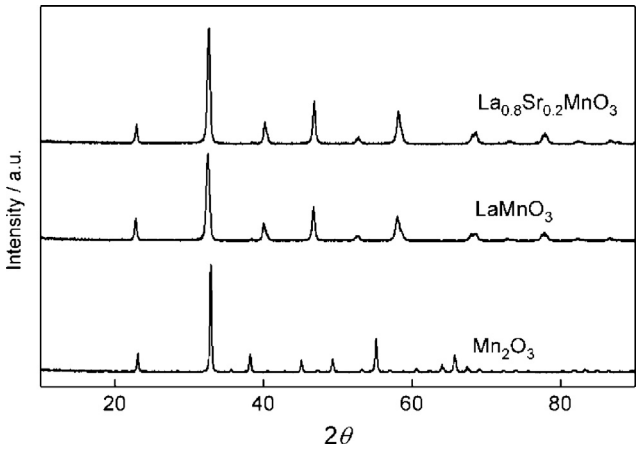

Fig. 3. XRD patterns of perovskite oxides and manganese oxides.

Table 3
Catalytic activities of manganese oxide and perovskite oxides for benzene oxidation with ozone.[a]

Catalyst	Reaction temperature (°C)	Benzene conversion (%)	CO mole fraction (%)	Ozone conversion (%)	Ozone/benzene decomposition	Surface area ($m^2\ g^{-1}$)
Mn_2O_3	70	80.0	26.7	76.8	13.9	14.4
	100	96.7	25.5	99.7	15.2	
$LaMnO_3$	70	16.4	23.5	19.7	17.6	15.7
	100	53.3	12.0	80.6	21.5	
$La_{0.8}Sr_{0.2}MnO_3$	70	30.5	16.7	28.3	17.3	17.6
	100	58.6	10.9	87.7	22.7	

[a] Catalyst 0.20 g, benzene 150 ppm, O_3 2250 ppm, O_2 10%, gas flow rate 500 ml/min (W/F = 0.4 g min l^{-1}).

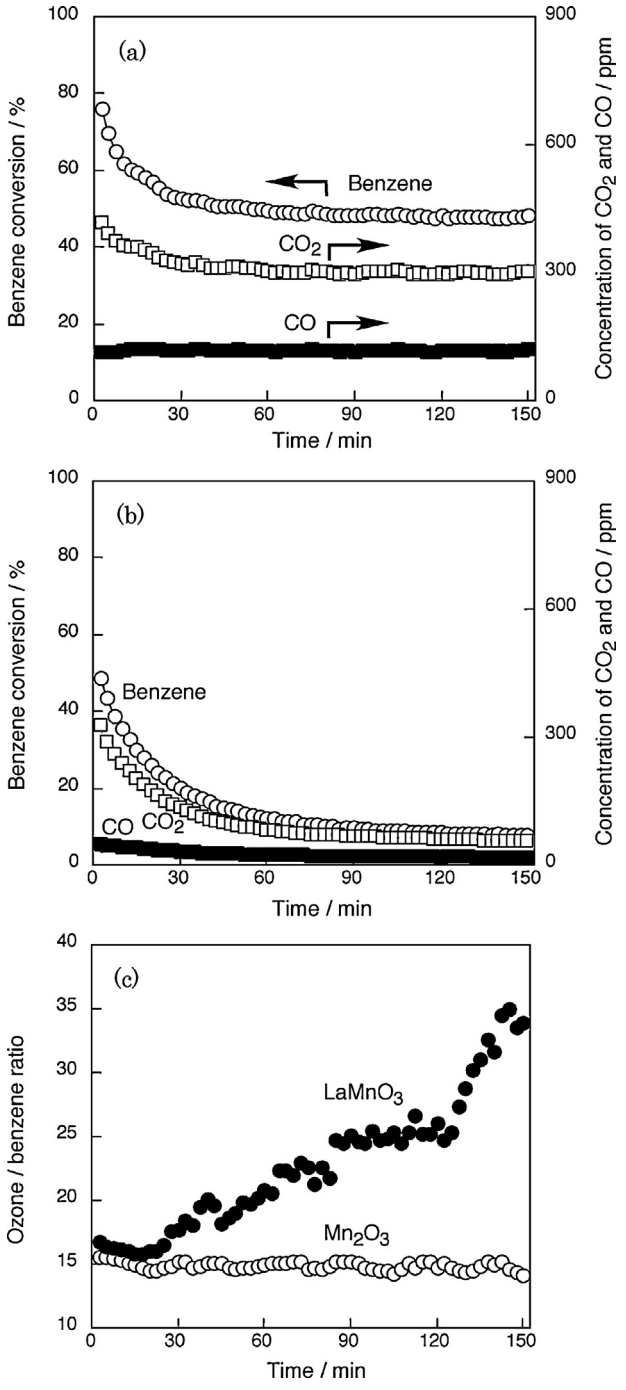

Fig. 4. Time course for benzene oxidation with ozone over and catalysts. (a) Benzene conversion with Mn_2O_3, and (b) with $LaMnO_3$. (c) Comparison of ozone/benzene ratio. Catalyst 0.10 g, inlet concentration: benzene 150 ppm, O_3 2250 ppm, O_2 10%, gas flow rate 500 ml/min (W/F = 0.2 g min l^{-1}), reaction temperature 70 °C.

that the substitution of Sr to A site of $LaMnO_3$ perovskite oxides enhanced the oxidation ability due to the changes in the Mn oxidation state [25]. In the case of catalytic ozonation of benzene, the Sr substitution slightly improved the catalytic activities, although the activity was still lower than that with Mn_2O_3. As the increase in reaction temperature, the CO mole fraction with perovskite oxides decreased and the ozone/benzene decomposition ratio increased, indicating that self-decomposition of ozone was promoted at elevated temperature. On the other hand, the CO mole fraction and ozone/benzene decomposition ratio for Mn_2O_3 catalyst did not depend on the reaction temperature.

Fig. 5 shows FTIR spectra of the Mn_2O_3 and $LaMnO_3$ catalysts used for benzene oxidation with ozone. The spectrum for the used $LaMnO_3$ exhibited the bands of oxygen-containing intermediates on the catalysts in the wavenumber range 1000–1800 cm^{-1}. The band at around 1644 cm^{-1} and the bands at around 1400 cm^{-1} can be the overlapping of several bands including the asymmetric and symmetric COO stretching of the surface carboxylates. The bands at 1186 and 1314 cm^{-1} were assignable to the CO stretching of alcohols, carboxylic acids, and esters. The band at 3300–3500 cm^{-1} was due to the stretching of OH groups of alcohols and carboxylic acids. The presence of these bands indicated that catalyst deactivation of $LaMnO_3$ in Fig. 4 was ascribed to the formation of strongly-bound compounds on the catalysts. The bands of oxygen-containing species were also observed on Mn_2O_3. However, the band intensities for the CO and COO groups were relatively lower and the band of OH groups at 3300–3500 cm^{-1} was absent on Mn_2O_3. The interaction between the catalyst surface and intermediate compounds for the Mn_2O_3 catalyst may be weaker than that

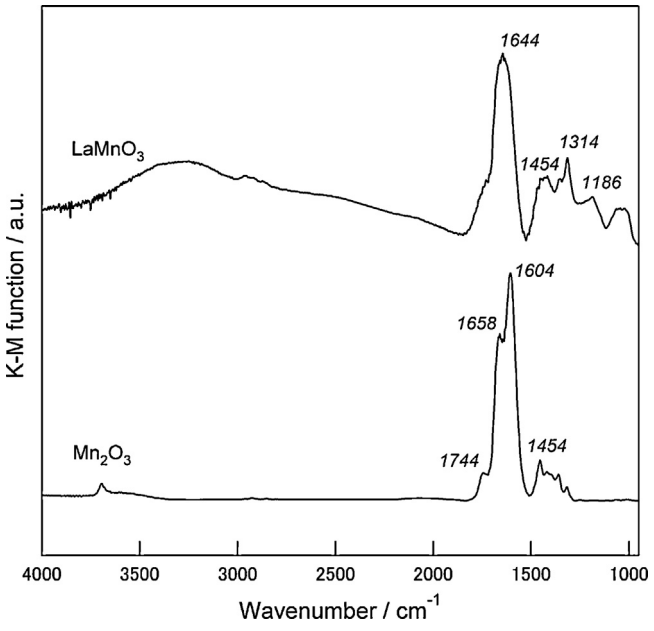

Fig. 5. FTIR spectra of intermediate compounds on Mn_2O_3 and $LaMnO_3$ catalysts.

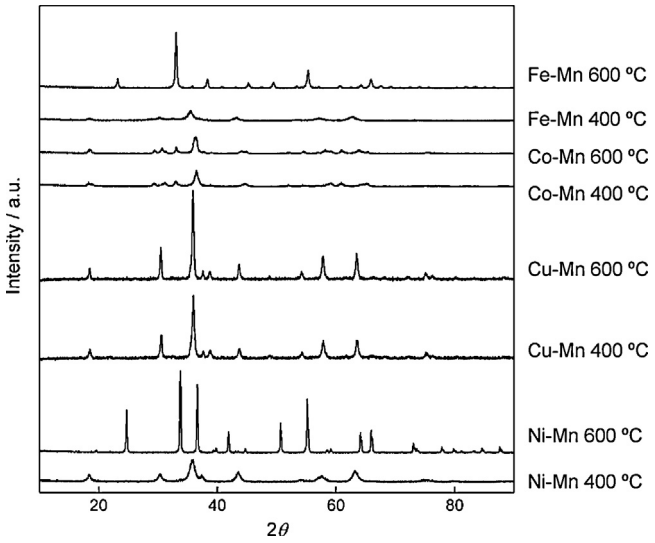

Fig. 6. XRD patterns of manganese-based mixed oxides.

for $LaMnO_3$ catalyst. When the used catalysts were heated with continuous ozone feed, the intermediate compounds were oxidized to CO_2. According to the profiles for CO_2 formation, the amounts of byproduct compounds were determined to be 3.57×10^{-4} C mol/g-catalyst and 2.88×10^{-4} C mol/g-catalyst for $LaMnO_3$ and Mn_2O_3, respectively. Thus, the amount of the byproduct compounds was larger for $LaMnO_3$ catalyst. These findings suggested that the presence of La on the catalyst promoted the accumulation of byproduct compounds which were strongly bound to the catalyst and more difficult to be decomposed than those on Mn_2O_3 catalyst.

3.3. Benzene oxidation behavior on manganese-containing mixed metal oxides

We have also investigated the catalytic properties of mixed metal oxides that contained Mn and other transition metals in the first transition series. Here, equimolar of transition metal nitrate (Fe, Co, Ni, and Cu) was combined with Mn nitrate for the preparation of mixed metal oxides by the AMP method. Fig. 6 shows the XRD patterns of the mixed metal oxides thus prepared. Distinct diffraction patterns for Cu–Mn spinel phases were observed for Cu–Mn oxides after calcination at 400 and 600 °C. For Ni–Mn catalysts, $NiMnO_3$ phase was clearly observed after calcination at 600 °C, whereas small peaks for Mn_3O_4 were mainly observed after calcination at 400 °C. Only Mn oxide phases were observed for Fe–Mn catalysts: Mn_3O_4 was detected after calcination at 400 °C and Mn_2O_3 was clearly observed at 600 °C. In the case of Co–Mn oxides, $CoMn_2O_4$ phase was observed along with Mn_3O_4 phases. Among the mixed oxides, Cu–Mn oxides calcined at 400 and 600 °C and Ni–Mn oxides calcined at 600 °C contained mixed oxide phases with high crystallinity.

EXAFS studies further revealed the structures of Mn-based mixed oxides. Fig. 7 shows the Mn-K edge EXAFS spectra of the mixed oxides prepared by AMP methods and calcined at 400 °C. Mn oxides exhibited the peak due to Mn–O in the first coordination shell and the peaks for Mn–Mn and Mn–O in the second coordination shell. The EXAFS spectra of Co–Mn, Cu–Mn, and Ni–Mn oxides were different from those of Mn oxides: the peak positions for Mn–O in the first coordination shell were similar, but the peak positions for the second coordination sphere were different. This indicates that the local structure around Mn atom was changed by the addition of transition metals to Mn oxides.

The Mn-containing mixed oxides exhibited steady-state activities for benzene oxidation with ozone at 70 °C. The benzene

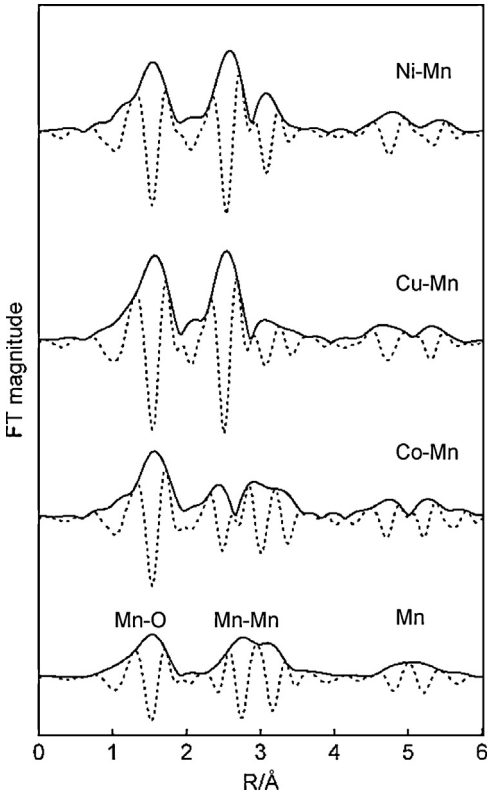

Fig. 7. Mn–K edge EXAFS spectra of manganese-based mixed oxides.

oxidation rate was plotted against catalyst surface area in Fig. 8. The surface area decreased by increasing the calcination temperature for mixed metal oxides, as in the case of Mn monoxides. The benzene conversion increased with increasing catalyst surface area for all the catalysts. The reaction rate for Co–Mn mixed oxides calcined at 600 °C was comparable with that for Mn monoxides. However, other mixed oxide catalysts exhibited lower activities. Cu–Mn and Ni–Mn oxides with high degree of crystallinity showed much lower surface area and lower activity than other mixed oxide catalysts.

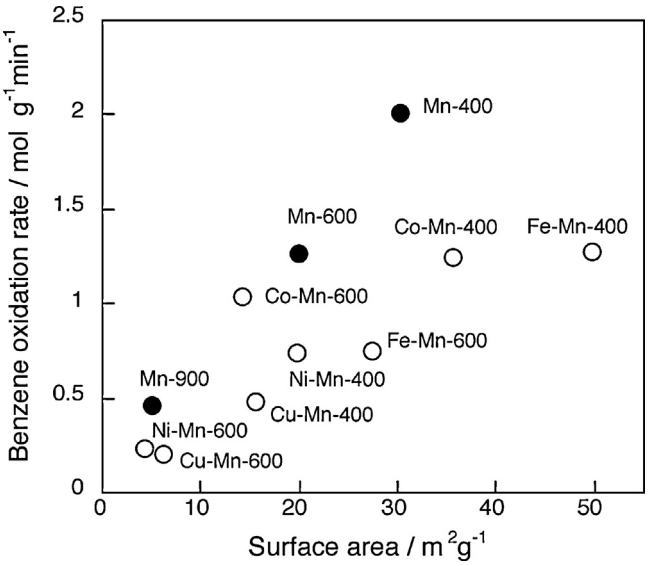

Fig. 8. Effect of surface area on benzene oxidation rate over Mn-containing mixed metal oxides. Inlet concentration: benzene 150 ppm, O_3 2250 ppm, O_2 10%, gas flow rate 500 ml/min, reaction temperature 70 °C.

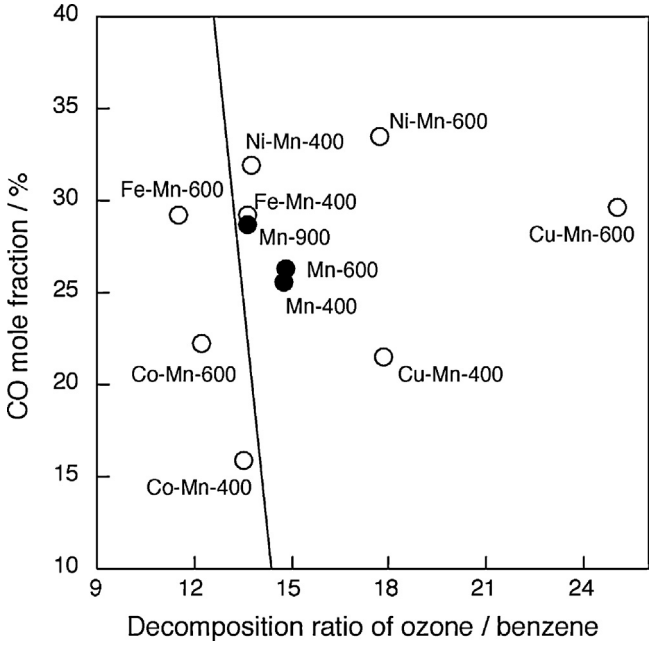

Fig. 9. Plots of CO mole fraction against decomposition ratio of ozone to benzene. Inlet concentration: benzene 150 ppm, O_3 2250 ppm, O_2 10%, gas flow rate 500 ml/min, reaction temperature 70 °C.

Although the addition of Fe to Mn oxides increased the catalyst surface area, the benzene oxidation activities were not improved. Thus, Mn-containing mixed oxides are ineffective in improving catalytic activities for benzene oxidation.

As described above, in the case of benzene oxidation with Mn monoxides, ozone/benzene decomposition ratio and CO mole fraction were independent of the catalyst calcination temperature. On the other hand, Mn-containing mixed metal oxides exhibited various values for CO mole fraction and ozone/benzene decomposition ratio. Fig. 9 shows the relationship between CO mole fraction and decomposition ratio of ozone to benzene. The Co–Mn and Cu–Mn mixed metal oxides calcined at 400 °C showed lower CO mole fraction than Mn monoxides. Comparison of these values with those obtained from stoichiometric equation (Eq. (5)) revealed the efficiency for ozone utilization in benzene oxidation with ozone. The solid line in Fig. 9 indicates the relationship between CO mole fraction and ozone/benzene mole fraction obtained from the stoichiometric equation. Therefore, the plots were close to the line when the reaction stoichiometrically proceeded. The CO mole fraction and ozone/benzene ratio were comparable for Fe–Mn oxides and Mn monoxides. The addition of Cu to Mn monoxides increased the ozone/benzene decomposition ratio, indicating that it promoted the self-decomposition of ozone. The CO mole fraction and ozone/benzene ratio for Ni–Mn oxides calcined at 400 °C were close to those for Mn oxides, whereas ozone/benzene decomposition ratio increased when Ni–Mn oxide calcined at 600 °C was used as the catalyst. The plots for Co–Mn mixed oxides were very close to the solid line and CO mole fraction was lower than that for Mn oxides. Thus, the Co–Mn catalysts are the effective catalysts from the standpoint of CO_2 selectivity and efficiency for ozone utilization.

Fig. 10 shows the formation behavior of CO_2 and CO and ozone/benzene decomposition ratio at various benzene conversion with Mn and Co–Mn oxide catalysts. Here, W/F value was variously changed to control the benzene conversion. Good relationship was observed between the amount of CO_2 and CO formed and that of benzene consumed for both catalysts (Fig. 10(a)), indicating that

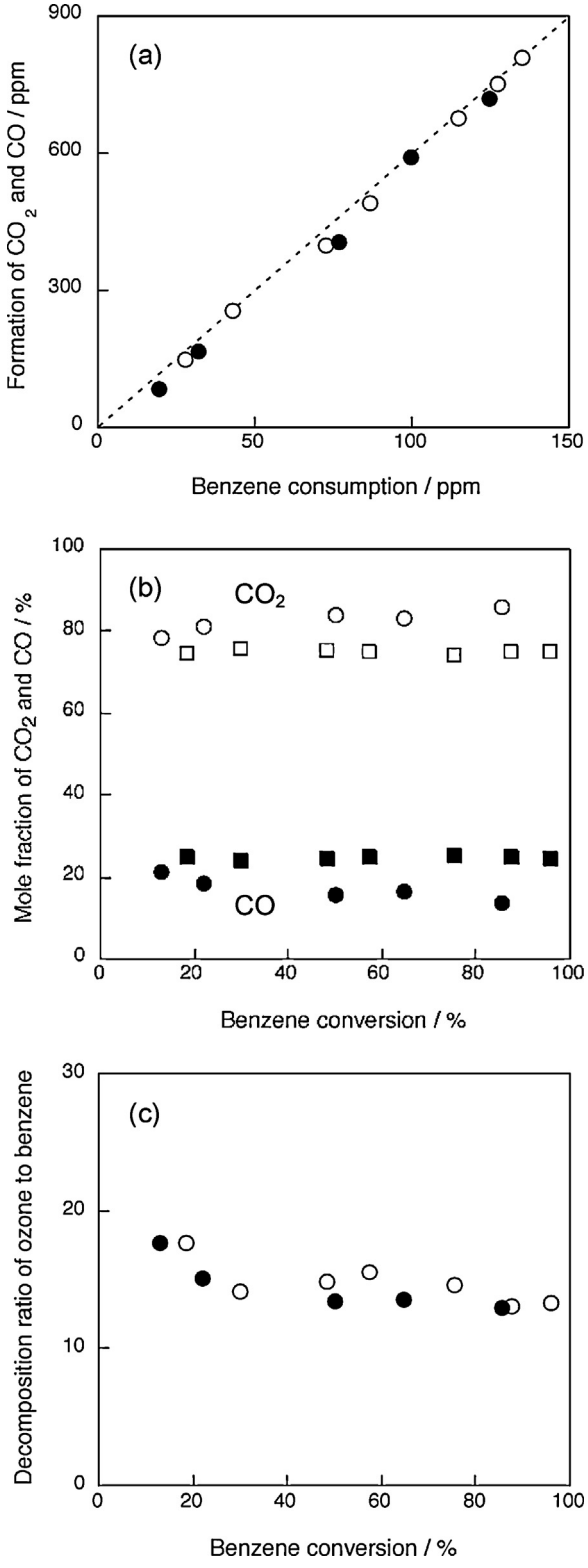

Fig. 10. Benzene oxidation behavior on Co–Mn and Mn oxide catalysts. (a) Relationship between benzene consumption and CO_x formation. (●) Co–Mn; (○) Mn. (b) relationship between benzene conversion and mole fraction of CO_2 and CO. Co–Mn (○, ●); Mn (□, ■). (c) decomposition ratio of ozone to ratio vs. benzene conversion. (●) Co–Mn; (○) Mn. Inlet concentration: benzene 150 ppm, O_3 2250 ppm, O_2 10%, reaction temperature 70 °C.

benzene was completely transformed to CO_2 and CO. As the benzene conversion increased, CO mole fraction decreased and CO_2 mole fraction increased (Fig. 10(b)) for Co–Mn catalyst, indicating that byproduct CO formed in benzene oxidation was oxidized to CO_2 on Co–Mn catalyst. In contrast, the mole fractions were almost independent of benzene conversion for Mn monoxide catalyst, indicating that the sequential oxidation of CO to CO_2 did not proceed with Mn monoxide catalysts under our reaction conditions (Fig. 10(c)). The ozone/benzene decomposition ratio was comparable for these two catalysts and almost independent of benzene conversion, although the values slightly increased at low conversion levels.

As shown in Fig. 8, benzene conversions with mixed oxides were lower than those with Mn oxides, whereas the surface areas of the Mn-containing mixed oxides were higher than those of Mn oxides. It is likely that ozone is decomposed on the Mn-containing mixed oxides to form the active oxygen species (O^*), which takes part in benzene oxidation (Eqs. (1) and (4)), as in the case of Mn oxides. The lower activities of Mn-containing mixed oxides than Mn oxides were ascribed to the build-up of byproduct compounds, which more strongly suppressed the formation of the active oxygen species on the mixed oxides, leading to the decrease in steady state benzene oxidation rate. Therefore, the addition of metal (Fe, Co, Ni, and Cu) to Mn oxides promoted the accumulation of less-reactive byproduct compounds on the catalysts. On the other hand, ozone/benzene decomposition ratios for Mn-containing mixed oxides except for Cu–Mn and Ni–Mn oxides were close to the stoichiometric values, indicating that ozone was efficiently consumed in benzene oxidation, in marked contrast with La-containing perovskite oxides. The addition of Co to Mn oxides improved their CO oxidation ability, and therefore increased the CO_2 mole fraction in benzene oxidation with ozone.

It should be noted that the Mn-containing mixed oxides prepared by RHP method with $NaHCO_3$ showed lower CO mole fraction and higher ozone/benzene decomposition ratio, which was almost the same trend with Mn oxides prepared by the same method. XRD studies clarified that Na-containing mixed oxides were formed in the mixed oxides, which promoted the self-decomposition of ozone on the catalysts.

4. Conclusion

In summary, this study revealed the effect of catalyst composition and preparation conditions on the catalytic properties of Mn-based oxides for benzene oxidation with ozone. Catalytic properties of Mn oxides were compared with those of Mn-containing mixed oxides from the standpoint of activity, product distribution (CO mole fraction) and the efficiency for ozone utilization (ozone/benzene decomposition ratio). The properties of Mn monoxides were independent of the two preparation methods, evaporation-to-dryness method and co-precipitation method. In the case of perovskite oxides, the addition of La had the detrimental effect on catalytic activity and efficiency for ozone utilization and it promoted the formation of strongly-bound intermediate compounds on the catalyst. The ozone/benzene decomposition ratio and CO mole fraction were variously changed when Mn oxides were combined with other metals in the first transition series (Fe, Co, Ni, and Cu). Co–Mn mixed oxides were one of the good candidates for benzene oxidation with ozone from the standpoint of CO_2 selectivity and efficiency for ozone utilization.

Acknowledgements

This work was financially supported by Steel Foundation for Environmental Protection Technology. This work was also supported by JSPS KAKENHI Grant Number 22560765.

References

[1] P. Hunter, S.T. Oyama, Control of Volatile Organic Compound Emissions: Conventional and Emerging Technologies, Wiley-Interscience, New York, 2000.
[2] A. Naydenov, D. Mehandjiev, Applied Catalysis A: General 97 (1993) 17–22.
[3] W. Li, G.V. Gibbs, S.T. Oyama, Journal of the American Chemical Society 120 (1998) 9041–9046.
[4] W. Li, S.T. Oyama, Journal of the American Chemical Society 120 (1998) 9047–9052.
[5] R. Radhakrishnan, S.T. Oyama, J.G. Chen, K. Asakura, Journal of Physical Chemistry B 105 (2001) 4245–4253.
[6] Y. Xi, C. Reed, Y.-K. Lee, S.T. Oyama, Journal of Physical Chemistry B 109 (2005) 17587–17596.
[7] C. Reed, Y. Xi, S.T. Oyama, Journal of Catalysis 235 (2005) 378–392.
[8] C. Reed, Y.-K. Lee, S.T. Oyama, Journal of Physical Chemistry B 110 (2006) 4207–4216.
[9] A. Gervasini, G.C. Vezzoli, V. Ragaini, Catalysis Today 29 (1996) 449–455.
[10] D. Andreeva, T. Tabakova, L. Ilieva, A. Naydenov, D. Mehanjiev, M.V. Abrashev, Applied Catalysis A: General 209 (2001) 291–300.
[11] D. Mehandjiev, A. Naydenov, G. Ivanov, Applied Catalysis A: General 206 (2001) 13–18.
[12] E. Rezaei, J. Soltan, Chemical Engineering Journal 198–199 (2012) 482–490.
[13] J.H. Park, J.M. Kim, M. Jin, J.K. Jeon, S.S. Kim, S.H. Park, S.C. Kim, Y.K. Park, Nanoscale Research Letters 7 (2012) 14.
[14] J.H. Park, J. Jurng, G.N. Bae, S.H. Park, J.K. Jeon, S.C. Kim, J.M. Kim, Y.K. Park, Journal of Nanoscience and Nanotechnology 12 (2012) 5942–5946.
[15] C.R. Lee, J. Jurng, G.N. Bae, J.K. Jeon, S.C. Kim, J.M. Kim, M. Jin, Y.K. Park, Journal of Nanoscience and Nanotechnology 12 (2011) 7303–7306.
[16] M. Li, K.N. Hui, K.S. Hui, S.K. Lee, Y.R. Cho, H. Lee, W. Zhou, S. Cho, C.Y.H. Chao, Y. Li, Applied Catalysis B: Environmental 107 (2011) 245–252.
[17] D.-Z. Zhao, C. Shi, X.-S. Li, A.-M. Zhu, B.W.-L. Jang, Journal of Hazardous Materials 239–240 (2012) 362–369.
[18] H. Einaga, S. Futamura, Reaction Kinetics and Catalysis Letters 81 (2004) 121–128.
[19] H. Einaga, S. Futamura, Journal of Catalysis 227 (2004) 304–312.
[20] H. Einaga, A. Ogata, Journal of Hazardous Materials 164 (2009) 1236–1241.
[21] M.A. Pena, J.L.G. Fierro, Chemical Reviews 101 (2001) 1981–2017.
[22] M.B. Gawande, R.K. Pandey, R.V. Jayaram, Catalysis Science & Technology 2 (2012) 1113–1125.
[23] D. Mehandjiev, K. Cheshkova, A. Naydenov, V. Georgesku, Reaction Kinetics and Catalysis Letters 76 (2002) 287–293.
[24] D.C. Koningsberger, Japanese Journal of Applied Physics, Supplements 32–2 (1993) 877–878.
[25] N. Yamazoe, Y. Teraoka, Catalysis Today 8 (1990) 175–199.